https://doi.org/10.20965/ijat.2021.p0696



Paper:

# Design, Fabrication, and Performance Analysis of a Vertically Suspended Soft Manipulator

**Mohamed Tahir Shoani*, Mohamed Najib Ribuan*,†, and Ahmad Athif Mohd Faudzi**,*****

*Faculty of Electrical and Electronic Engineering, Universiti Tun Hussein Onn Malaysia (UTHM)
Parit Raja, Batu Pahat, Johor 86400, Malaysia
†Corresponding author, E-mail: mnajib@uthm.edu.my
**School of Electrical Engineering, Faculty of Engineering, Universiti Teknologi Malaysia (UTM), Skudai, Malaysia
***Center for Artificial Intelligence and Robotics, Universiti Teknologi Malaysia (UTM), Kuala Lumpur, Malaysia
[Received October 9, 2020; accepted December 21, 2020]

**Soft continuum manipulators are comprised of flexible materials in a serpentine shape. Such manipulators can be controlled mechanically through tendons or pneumatic muscles. Continuum manipulators utilizing tendons are traditionally formed in a thick cross section, which presents limitations in achieving a high bending range as well as difficulties for storage and transportation. This study introduces a continuum manipulator comprised of two thin plastic bands and driven by a tendon to provide a bending action. The manipulator's thin body form enables it to be rolled up for storage and transportation. Experimental results on different section lengths show the possibility of achieving a horizontal displacement of up to 34% of the bending-segment's length, and a full closed-loop curvature for most segments. However, the results also indicated an elongation of the tip paths owing to gravity. These results, in addition to the manipulator's flexibility and light weight features, confirm its suitability for applications in space and underwater environments.**

**Keywords:** soft robotics, tendon-driven, continuum structures, manipulator

## 1. Introduction

Soft robots are comprised of soft or flexible materials [1]. Compared to rigid robots, soft robots provide safe human interaction, high dexterity, and the ability to handle irregular objects [2–4]. Soft continuum manipulators [5–7] feature a continuous curvilinear body allowing them to adjust to unstructured environments and locations of continuous curvature, such as in search and rescue [8] or medical operations [9, 10].

Continuum manipulators can be driven using fluidic [11–14], shape memory alloy (SMA) [15, 16], mechanical [17, 18], or tendons actuators [19–21]. While fluidic actuators are soft and relatively safer for direct human interaction, they require a compressor and hoses to provide the pressurized fluid, making the system bulky and reducing its range of applications. SMA provides a high force and can be used in miniature sizes; however, it requires relatively high temperatures to enable its state transition and the extent of actuation (extension or retraction) is more difficult to control. Mechanical actuation utilizing concentric pre-curved tubes enables manipulators with very small diameters to be used to penetrate the human body in minimally invasive surgery and other industrial applications; however, their workspace is aimed at their distal end rather than the entire length of the manipulator's arm. Although tendon actuation works in one way (retraction) and requires a second tendon or other means to counter its operation, it provides accuracy, mobility, large workspace coverage, and the potential to work in most environments. These attributes make tendons an attractive option for soft manipulators.

Continuum manipulators are commonly formed with a circular cross-section [22–25] as it provided the ability to uniformly operate in a three-dimensional space. However, employing different body forms can introduce new abilities and applications. The thin body form demonstrates higher bendability, a smaller storage reel radius, and a better ability to resist a lateral bending force normal to the body's wider dimension. A body form of this type was presented in [26], where it was operated horizontally, thus limiting the effect of gravity. However, the manipulator used McKibben actuators, which require the availability of a compressor, thus making it less suitable for mobile or space applications. In [27], a manipulator was controlled with tendons and utilized a backbone of six flat springs. The springs enabled the manipulator to bend in one direction while possessing high passive stiffness in the orthogonal direction. However, owing to its overall circular cross-section, the manipulator could only reach a maximum bending angle of 143°.

This paper introduces a tendon-driven, vertically suspended continuum manipulator with a wide body and thin cross-section. This configuration enables the manipulator to reach a 360° bending, thus possessing greater flexibility for inspection and object retrieval tasks in space. This can be accomplished using a camera for inspection and a hook or gripper to grasp the item of interest. The item can then be retrieved when the tendon is retracted, causing the



© Fuji Technology Press Ltd. Creative Commons CC BY-ND: This is an Open Access article distributed under the terms of the Creative Commons Attribution-NoDerivatives 4.0 International License (http://creativecommons.org/licenses/by-nd/4.0/).

manipulator tip, hence the gripper, to be pulled back to the manipulator's base. In contrast to rigid manipulators, the soft body of the manipulator makes it less vulnerable to collisions by space junk or other objects in the environment. Another possible application is in agriculture for grain manipulation in storage bins. In contrast to rigid solutions, the soft manipulator would be safe to nearby personnel who can work in proximity without fear of injury in case of collision with the manipulator. This study attempts to establish a relationship between the retracted tendon length and the planar displacement of the manipulator's tip, and then to validate the relationship through practical experimentation.

The remainder of this paper is organized as follows. Section 2 presents the mathematical modeling based on the predicted response of the manipulator. Section 3 focuses on the design, fabrication, and operation of the manipulator and provides an overview of its configuration. Section 4 provides an overview of the experimental setup, procedure, and results. Section 5 discusses the outcome of the experiments and presents an analysis of the differences between the predicted and measured readings. Finally, Section 6 provides conclusive remarks on the work and prospects for future research in this field.

## 2. Manipulator Model

The continuum manipulator is held in a vertically suspended position with its base fixed at the top, and its tip free at the lower end. This arrangement is more suitable for soft continuum manipulators because the force of gravity causes them to collapse if aligned in any other configuration.

For each side, a tendon was attached to the manipulator's tip at the lower end, and it entered the manipulator's body through a hole (inlet) at a specific distance from the tip. The point of entry is considered a tendon attachment point as retraction of the tendon through it causes the manipulator tip to bend toward that specific entry point.

The manipulator body contains five inlets, and the tendon can be routed through any one of them. The radius of the manipulator's workspace is directly proportional to the bending segment's length, which is determined by the distance of the inlet from the arm's tip (lower). To calculate the manipulator's tip displacement for any inlet, a model was used, as shown in **Fig. 1**. In this model, $L$ denotes the manipulator's length, $a$ denotes the length of the tendon from the inlet to the tip of the manipulator, $b$ denotes the tip's horizontal displacement, $c$ denotes the height of the triangle $abc$, which is also the difference between the non-retracted tendon length $L_2$ and the tip's vertical displacement $d$.

Initially, at the rest position, the tendon length from the lower tip to the inlet is equal to $L_2$; thus,

$$L_2 = d + c. \quad \ldots \quad (1)$$

When the tendon is retracted, it generates an angle $\theta$ between itself and the vertical line representing the manipulator at rest. Thus,

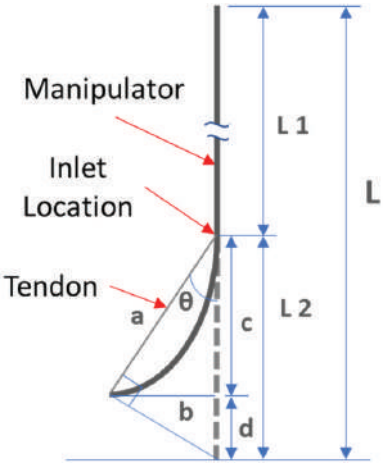


**Fig. 1.** Illustration of the manipulator in bending posture.

$$a = L_2 \cos\theta, \quad \ldots \quad (2)$$

$$b = a \sin\theta, \quad \ldots \quad (3)$$

$$c = a \cos\theta. \quad \ldots \quad (4)$$

Using Eq. (1) and substituting for $c$, $d$ is obtained as follows.

$$d = L_2 - a \cos\theta. \quad \ldots \quad (5)$$

In Eq. (3), $b$ represents the displacement in the $X$-direction, and in Eq. (5), $d$ represents the displacement in the $Y$-direction. Using Eqs. (3) and (5), two graphs can be drawn to show the expected horizontal ($x$-axis) and vertical ($y$-axis) displacements of the manipulator tip with respect to the tendon's length, passing through the five inlets. The two graphs are depicted in **Figs. 2(a)** and **(b)**.

## 3. Manipulator Design, Fabrication, and Operation

### 3.1. Manipulator Design

The manipulator's design comprised two thin flexible bands that were joined with small bolts through holes in the soft arm's body at the base (upper) and tip (lower). The use of two bands in a back-to-back configuration offsets the effect of the precurvature caused by the curling of the bands as a roll during storage. The tendons started from the manipulator's tip, ran externally, and then entered the body at one of several points. After entering the body, each of the two tendons continued internally upwards and exited through a separate hole in the base joint. Each tendon continued over a routing pulley towards the corresponding stepper motor. Finally, the tendon was attached to the pulley on the motor's shaft, which could rotate to extend or retract the tendon. The part of the manipulator's soft arm between its tip and the tendon's inlet is referred to as an arm-section. As mentioned earlier in Section 2, the entry points (inlets) in the manipulator body act

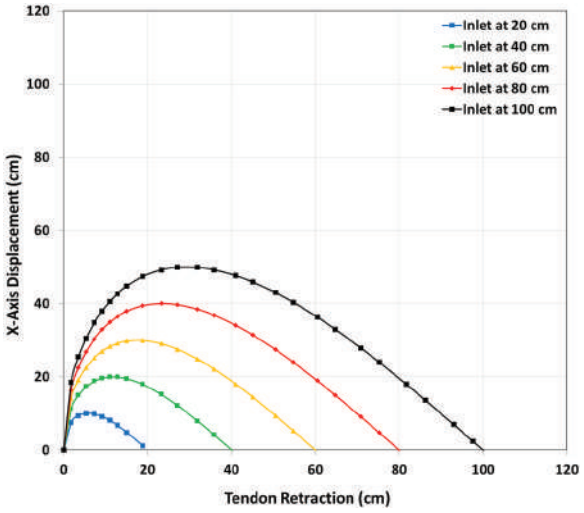


(a)

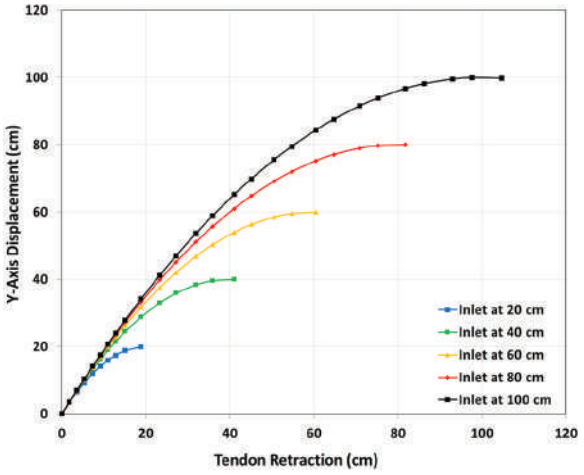


(b)

**Fig. 2.** Expected (a) horizontal and (b) vertical displacements of the manipulator's tip with respect to tendon retraction, for the five inlets.

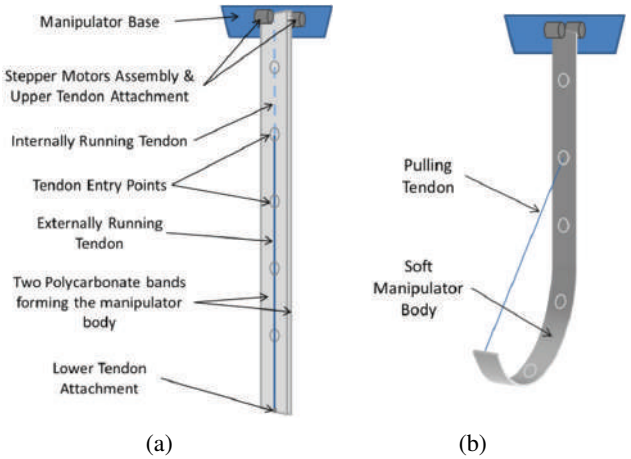


(a) (b)

**Fig. 3.** (a) Manipulator configuration and (b) manipulator in bending posture.

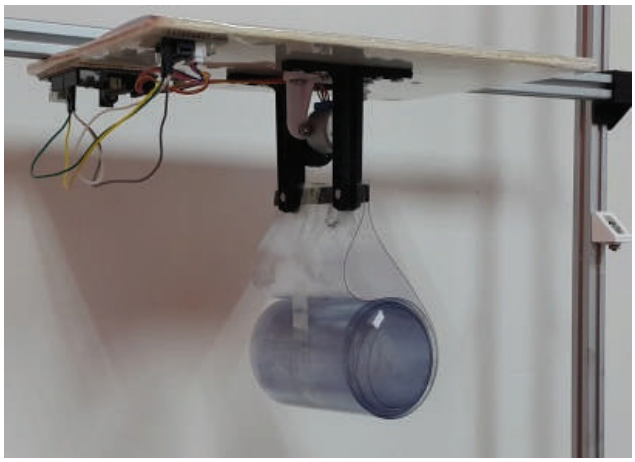

**Fig. 4.** The manipulator's arm in a rolled-up configuration.

as tendon attachment points, causing the pulled tendon to induce a curvature in the manipulator body as illustrated in **Figs. 3(a)** and **(b)**, which demonstrates the bending action owing to tendon retraction through the fourth inlet. Additionally, the manipulator's thin body facilitated curling it into a small compact form for transportation or storage purposes, as illustrated in **Fig. 4**.

### 3.2. Manipulator Fabrication

The fabrication of the manipulator started by preparing the long arm from a large polycarbonate sheet of 0.4-mm thickness. Two bands were cut from the sheet, each with a length of 110 cm and a width of 10 cm. The two bands would later be suspended next to each other to neutralize the effect of material-memory (residual) curvature, which is typical of sheets stored in a rolled form. Subsequently, several holes were made into the two polycarbonate bands. The holes had a diameter of 5 mm and were placed 20 cm apart, with the first one being 20 cm from the front end of the band. **Fig. 5** depicts a band with holes in the body.

Next, the tip of the manipulator was designed with one hook on either side to facilitate the tendon's attachment and detachment when a different inlet is to be selected. In addition, two openings, one in the front and another at the back, were made to accommodate an LED and a laser emitter, respectively. The LED faced forward to increase visibility, whereas the laser emitter would shine a red dot on the background, signifying the location of the tip, thus facilitating displacement measurements. **Fig. 6** illustrates the arm tip of the manipulator during the operation.

Finally, the top-side joint of the manipulator arm was fabricated. This consisted of four L-shaped brackets and a separator. The separator contained both vertical and horizontal holes. The vertical holes allowed the tendons to pass through from the arm towards the routing pulleys, whereas the horizontal holes were used to secure the manipulator arm to the holding brackets using screws. **Fig. 7** depicts the top-side assembly of the manipulator.

This arrangement was fixed to a wooden base at the top, which was bolted to the aluminum frame. The mi-

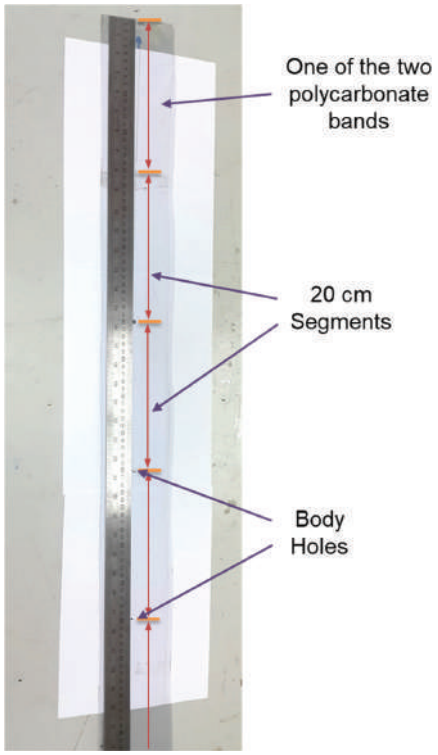


**Fig. 5.** Preparation of a manipulator arm band.

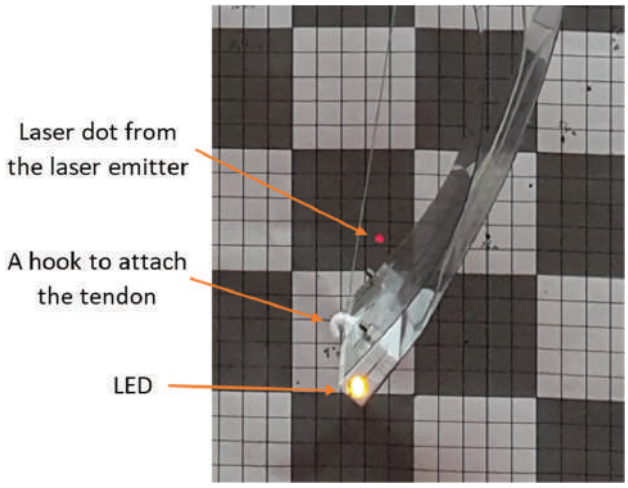


**Fig. 6.** The arm's tip with an LED in front and a laser dot from the laser emitter at the back.

crocontrollers, stepper motors, and driving boards were placed on a wooden base. The microcontrollers and driving boards were placed on top to facilitate connectivity and visual checking, whereas the stepper motors and conveying pulleys were placed on the underside to simplify tendon routing and control.

### 3.3. Manipulator Operation

The control of the manipulator was initiated at the PC, where the direction of rotation and number of revolute degrees were issued to the microcontroller. The received

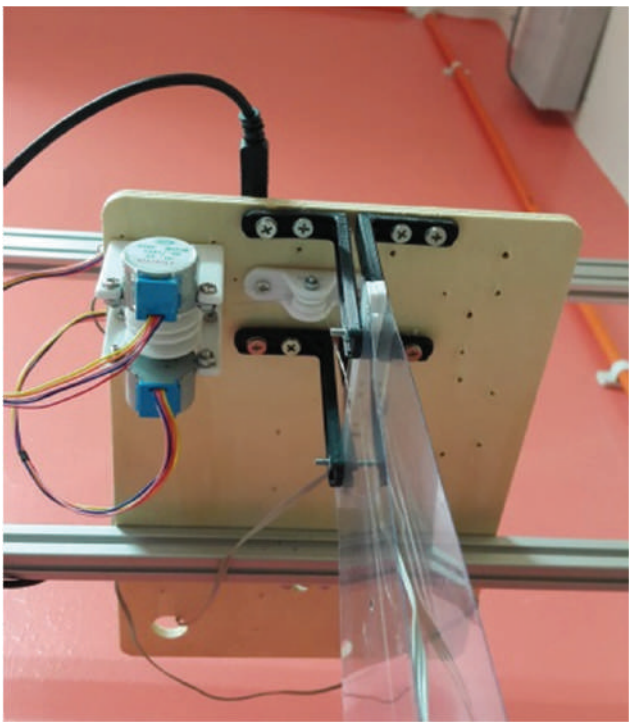

**Fig. 7.** The manipulator: base assembly.

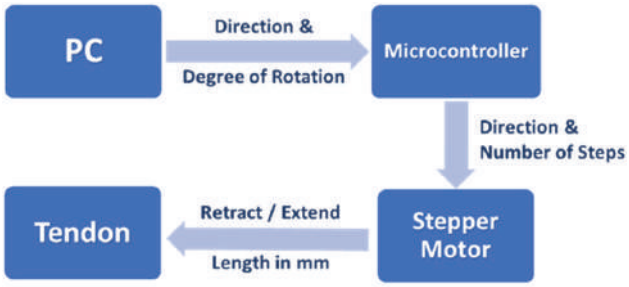


**Fig. 8.** Flow of control and information during the manipulator's operation.

data were converted by the microcontroller to a direction-of-rotation and number of motor-steps, and then passed to the stepper motors, as illustrated in **Fig. 8**. Finally, the stepper motors turned to pull or release the tendon, causing the manipulator arm to bend or straighten, as shown in **Figs. 3(b)** and **(a)**. The motor's release of the tendon causes the manipulator's arm to return to its default (straight) position owing to gravity and the manipulator body's elasticity. In the absence of gravity, the force of the body's elasticity might be insufficient to straighten the manipulator's arm in the presence of a relatively large force, such as friction, or a load that exceeds the force of the arm's elasticity.

By pulling the tendon, the manipulator could bend to reach any point in its path. For points outside the path, the tendons could be routed through a different inlet to allow for a different path. Currently, the manipulator body contains five inlets; however, new inlets can be easily in-

**Table 1.** Manipulator specifications.

| Attribute/Item | Dimension/Description |
|---|---|
| Total length | 110 cm |
| Bendable length | 108 cm |
| Width | 10 cm |
| Thickness | 0.4 mm per band = 0.8 mm |
| Number of bands | 2 |
| Material type | Polycarbonate plastic |
| Tendon type | Fishing line – 20 kg strength |
| Tendon supplier | DAISO Japan |
| Tendon diameter | 0.35 mm |
| Pully diameter | 19.1 mm |
| Motors | 2 × Stepper 28BYJ-48 |
| Motor controllers | 2 × ULN2003 |
| Brand of motors and motor controllers | China |
| Microcontroller | Arduino Uno |

troduced to the thin, soft body, allowing additional paths to reach any point within the manipulator's workspace to match the relevant application. **Table 1** lists the components and specifications of the manipulator.

The manipulator utilized an open-loop control approach. To reach any specific point in its workspace, the controller used Eqs. (3) and (5) to determine the required length of the tendon to reach that point. The motor was then rotated to pull or release the tendon accordingly, using the following equation to calculate the required rotation:

$$A_s = 180\frac{L_C}{\pi r}, \quad \ldots\ldots\ldots\ldots\ldots\ldots \quad (6)$$

where $A_s$ denotes the stepper motor's rotation angle in degrees, $L_C$ denotes the change in the tendon's length in millimeters, and $r$ denotes the radius of the pulley at the motor's shaft, which is 9.55 mm.

Although the stepper motor required some time to complete the retraction or release of the tendon, its driving board would not initiate a new rotation operation until the current operation was completed. Hence, issuing a new command to the stepper motor to retract or extend the tendon would only be executed once the current command was fulfilled. The time requirements for fulfilling a specific command depended on the rotational speed of the motor and the number of degrees to be rotated.

## 4. Experiment Details

An experiment was conducted to measure the response of the manipulator to tendon retraction through different inlets into the manipulator body.

Five inlets (holes) were made at 20, 40, 60, 80, and 100 cm from the lower tip of the manipulator. The data gathered from the experiment indicated the manipulator's behavior and its correlation with the model and calculated theoretical data.

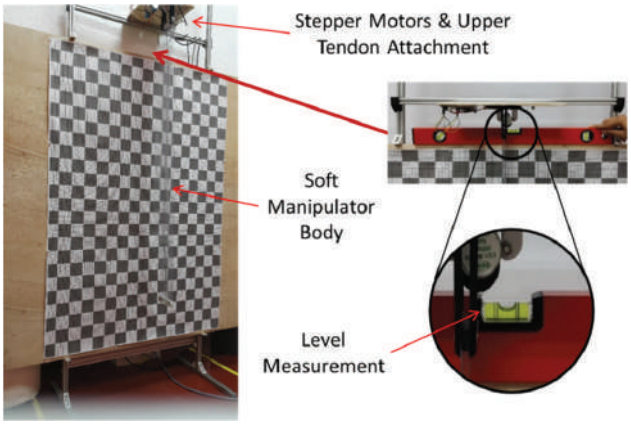


**Fig. 9.** Experimental setup showing the horizontal level verification of the manipulator base.

### 4.1. Setup and Calibration

To set up the experiment, the manipulator was attached to an aluminum frame such that it was vertically suspended, thus allowing the arm to bend without collapsing because of gravity. A checkered sheet was affixed to a wooden board, which was then attached to the same aluminum frame to serve as a background, thus assisting in obtaining measurements. The checkered background of 5-cm squares and 1-cm gridlines facilitated obtaining measurements during the experiment. The alignment of the manipulator and aluminum frame was verified with a level tool to ensure unbiased readings caused by misalignment. **Fig. 9** demonstrates the experimental setup and levelling verification.

### 4.2. Experiment Procedure

Initially the manipulator was at the default position (no bending; $\theta = 0°$). **Fig. 1** shows the location of $\theta$, whereas **Figs. 3(a)** and **9** (left) depict the manipulator in the default position. The starting point tip location $(0,0)$ was marked. Prior to starting the experiment, the stepper motors were rotated to tighten the tendon, thereby avoiding false readings caused by slack tendons. The tightening operation was conducted in two steps. First, the tendons were sufficiently retracted until sagging was eliminated. Each tendon was then retracted in steps of 1 mm. This was achieved by rotating the respective stepper motor by 6° for each step. The steps for the finer tightening continued until bending initiated, as indicated by the manipulator's tip deviation from the default $(0,0)$ position. At that point, the final 1-mm retraction step was reversed to return the arm to the default position while ensuring that the tendon was at its tightest attitude.

The experiment started by rotating the stepper motor by 90°, resulting in a 1.5-cm retraction of the tendon and a slight bending in the manipulator's arm. Then, the new location of the manipulator tip was recorded. This process

(pulling the tendon and recording the new measurement) was repeated until the manipulator's tip revolved, forming a closed loop and the tip touching the body. The illustration in **Fig. 1** shows the posture of the manipulator arm when it bends because of tendon retraction during the experiment.

The same procedure was followed for all the inlets. However, for the 20-cm inlet, the tip continued to translate vertically and did not revolve towards the body; hence, the measuring process continued until the tip reached a vertical displacement similar to the 1-m inlet iteration. The measurement process was repeated three times for each inlet to verify consistency.

### 4.3. Experiment Results

The motion of the manipulator is two-dimensional, and an experiment was conducted to determine the relationship between the length of the retracted tendon and the planar displacement of the manipulator's tip. In addition to using 1-cm gridlines, millimeter measurements were taken with a ruler to determine the exact displacements of the manipulator tip for each point. The measurements were then tabulated, and relative graphs were drawn.

Although tendon retraction was relatively slow, small oscillations were observed. Measurements were taken once the manipulator arm was stabilized to support repeatability. The experiment was repeated three times for each specific inlet (tendon entrance) in the manipulator body. Based on the average measurement of the three iterations, **Figs. 10(a)** and **(b)** depict the horizontal and vertical displacements of the manipulator with respect to the tendon retraction, respectively. **Figs. 11(a)** and **(b)** illustrate a comparison between the expected and measured horizontal and vertical displacements. For clarity, the data of only three arm-sections are presented.

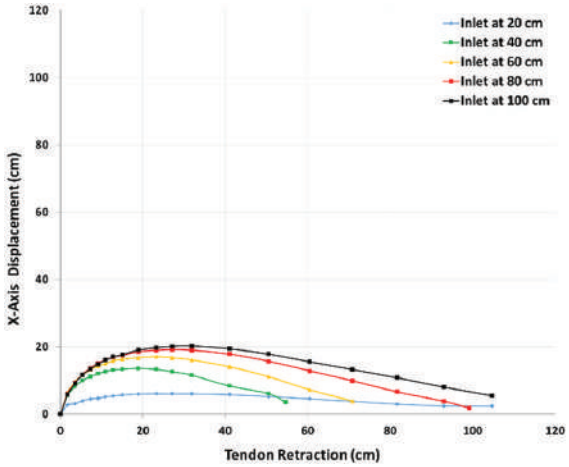


(a)

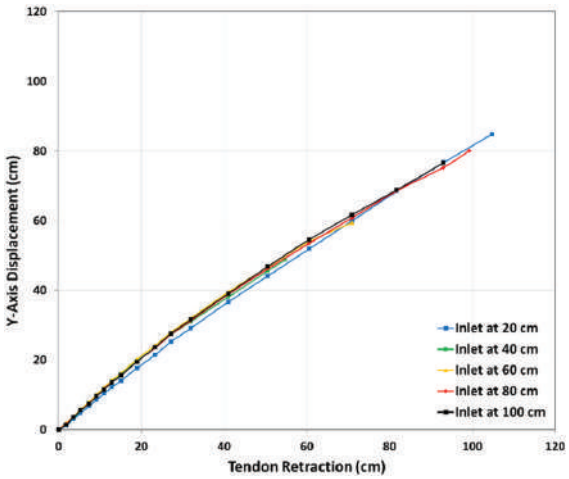


(b)

**Fig. 10.** Measured (a) horizontal and (b) vertical displacements of the manipulator's tip for the five inlets.

## 5. Analysis and Discussion

In this study, the response of a soft manipulator was measured, and the obtained results were presented in several graphs. Comparing the results, a correlation could be observed between the values predicted by the theoretical model and the practical (measured) ones, as shown in **Figs. 11(a)** and **(b)**. In **Fig. 11(a)**, both theoretical and practical values display a sharp increase in the beginning and a gradual decrease towards the end. In **Fig. 11(b)**, both values show a linear increase in the beginning but a non-linear overall curve.

However, the theoretical and practical values were not identical. By further examining the results, additional observations can be made. In the following sections, these observations are discussed, the differences between the calculated and measured readings are analyzed, and arguments and plausible causes are provided to justify the differences found.

### 5.1. Full Curvature

The inspection of the manipulator's response in **Fig. 10(a)** revealed that the graphs for arm sections larger than 20 cm showed a direction towards full revolution, indicated by their course towards crossing the $X$-axis at $y = 0$. However, it was also noted that the tip did not reach the full 360° curvature as the graphs stopped short of crossing the $X$-axis. This performance was caused by the flexibility and behavior of the two bands forming the manipulator body.

Because the arm bands were only tied together at the ends, the tendon pulled the body of the closer band towards the arm tip at the body-inlet, which caused the arm to form a closed loop at a deviated location with respect to $x = 0$. This deviation was inversely proportional to the distance from the upper base of the arm, as shown in **Figs. 12(a)** and **(b)**, where the deviation was larger for the 60 cm segment than for the 100 cm segment. Notably, because of the translucent color of the arm bands and to improve clarity, the edges of the manipulator arm are highlighted in **Figs. 12** and **13**.

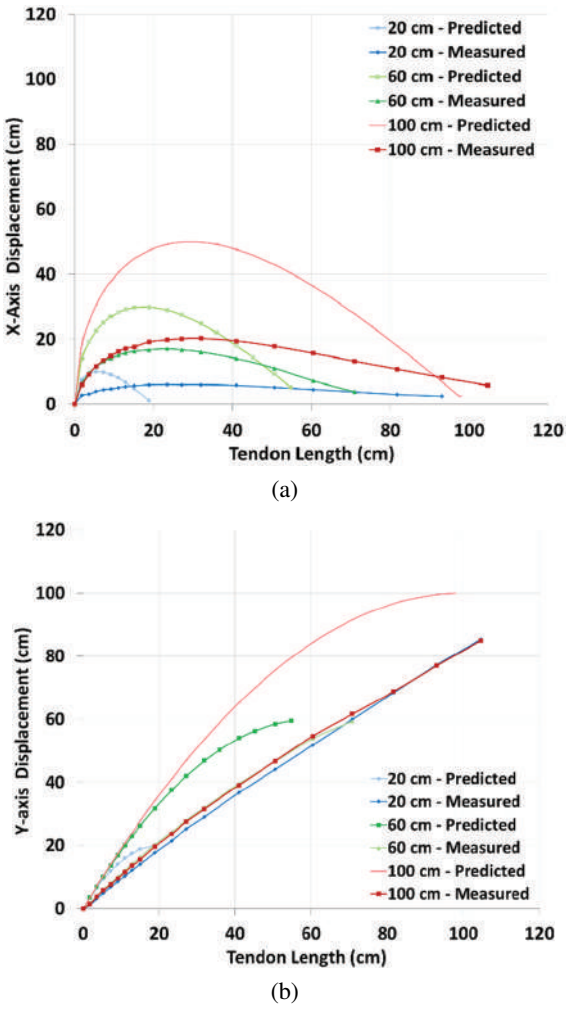


**Fig. 11.** Comparison of the predicted and measured displacements of the manipulator tip. (a) Horizontal. (b) Vertical.

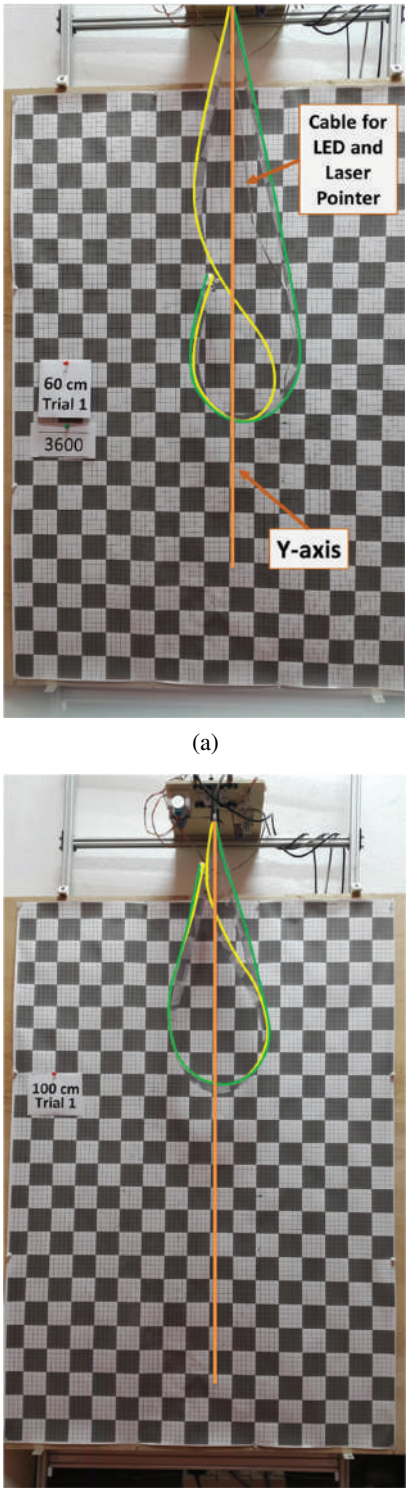


**Fig. 12.** Full curvature pattern of the manipulator arm. (a) Through 60-cm inlet. (b) Through 100-cm inlet.

## 5.2. Manipulator Tip Path Distortion

By inspecting the path of the manipulator's tip in **Fig. 10(a)** for the 20- and 40-cm segments, two types of distortions could be observed. The first type was related to the extreme elongation of the path for the 20-cm arm-section, whereas the second was an abnormal inverse curvature in the path of the 40-cm section in the vicinity of the $x = 40$ cm mark.

These distortions could be largely attributed to the difference in the deformation patterns of the two polycarbonate bands comprising the actuator, as shown in **Fig. 13(a)**. The difference in the bending pattern was a direct result of the disengagement of the two bands along the manipulator body. However, as the tendon entry points become farther from the tip, the body-disengagement effect decreased; hence, a more consistent path emerged, as depicted in **Fig. 13(b)**.

## 5.3. Reduction of Horizontal Displacement

Several observations were made during the comparison of the predicted values to the practical measurements. As shown in **Fig. 11(a)**, a reduction in the horizontal displacement (in the direction of the $X$-axis) of the manipulator tip was observed for all segments. For all the inlets larger than 20 cm, it was observed that the reduction increased as the tendon entry point became farther from the tip. The curve pertaining to the 60-cm arm-

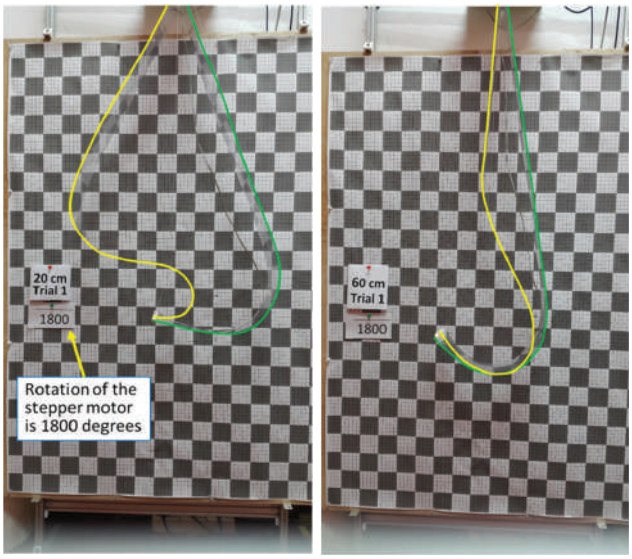


(a) Inlet at 20 cm (b) Inlet at 60 cm

**Fig. 13.** Different bending patterns of the two bands forming the manipulator body.

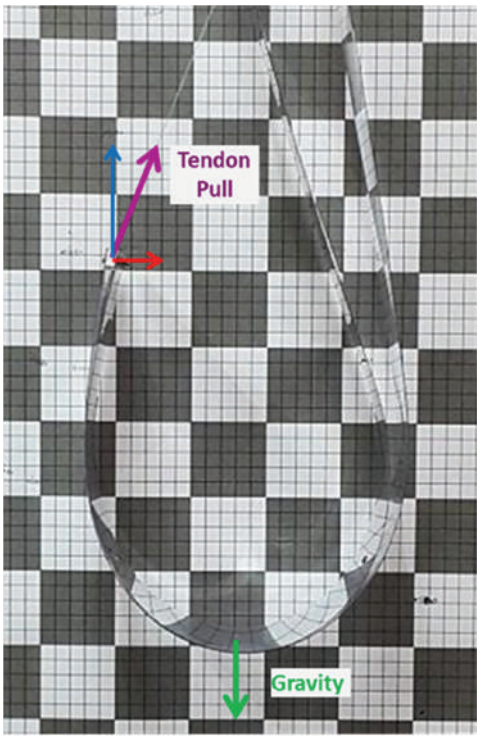


**Fig. 14.** Forces acting on the manipulator's tip.

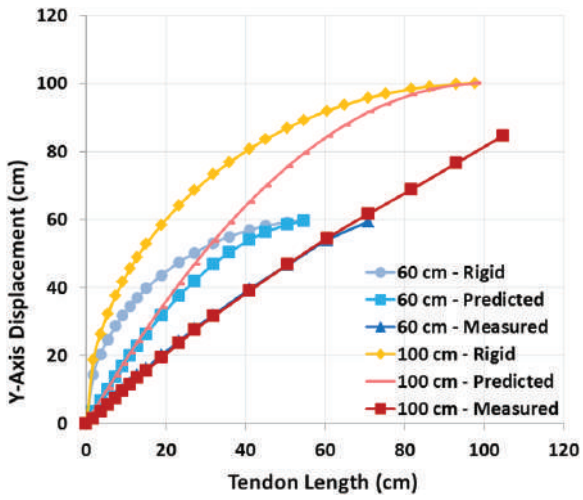


**Fig. 15.** Comparison of a rigid, predicted-soft, and measured-soft (under gravity) displacements of the manipulator tip in the vertical ($Y$-axis) direction.

section deviated by approximately 13 cm (43% reduction), whereas the curve of 100-cm section deviated by approximately 30 cm, representing an almost 60% reduction in the horizontal displacement.

This reduction in the horizontal displacement of the manipulator's tip was mainly caused by two factors. The first is the effect of gravity, which pulled the body downward, thus affecting the path's uniformity and causing it to elongate, thereby reducing the horizontal displacement. Because larger segments were heavier, they were affected more by gravity, and hence produced a shorter horizontal displacement.

The second factor for the reduction in the horizontal displacement was the horizontal force component resulting from the retraction of the tendon, as shown by horizontal arrow in **Fig. 14**. This component pushed the entire manipulator body in the direction opposite to that desired, thus reducing the horizontal displacement.

It can be assumed that utilizing a less flexible body could result in a better tolerance towards the force of gravity; however, such research is beyond the scope of the current study and could be further investigated in future work.

### 5.4. Linear Relationship of Vertical Displacement

**Figure 10(b)** shows a linear relationship between tendon retraction and the vertical displacement of the arm's tip. This, however, was different with respect to the expected values shown in **Figs. 2(b)** and **11(b)**, where the graph was initially linear, but towards the end. This difference could be largely attributed to the effects of gravity and the material's modulus of elasticity.

As shown in **Fig. 15**, for a rigid material with a relatively high modulus of elasticity, and where gravity had little effect, the graph represented a circular arc according to the following equation.

$$y = L_2 \sin\theta, \quad \ldots\ldots\ldots\ldots\ldots\ldots \quad (7)$$

where $y$ denotes the displacement in the vertical ($Y$-axis) direction, $L_2$ denotes the length of the arm, and $\theta$ denotes the deflection angle of the tendon. This equation slightly differs from Eq. (3) in Section 2 as the tendon length $a$ is replaced with the arm length $L_2$ because a rigid structure would have a negligible change in length when pulled by

the tendon in contrast to the soft body that bends due to tendon retraction.

## 6. Conclusion

In this study, a thin and relatively wide manipulator was introduced, utilizing tendons as a control mechanism for bending the soft body, thus achieving horizontal and vertical displacement. The manipulator's light weight and ability to be wound into a small roll makes it ideal for storage and transportation to remote locations. Additionally, the manipulator's configuration allows for the effortless fabrication of much longer versions of the same manipulator to suit related applications in space or underwater environments.

The performance of the manipulator was tested for each of the five inlets in the manipulator's body, which also act as tendon attachment points, and the results demonstrated the manipulator's ability to reach a horizontal displacement as far as the length of the bending segment. The results also confirmed the manipulator's ability of a full 360° curvature and thus, the ability to inspect the ceiling of the vertical structure. However, the results also highlighted some areas of improvement with respect to the effect of gravity on the soft body of the manipulator. In addition, the current research utilized specific inlets' locations in the manipulator's body to obtain specific bending section lengths. It would be interesting for future research to explore the possibility of upgrading the current configuration to a variable bending length, thus automating the process of adjusting the segment's length.

**Acknowledgements**

The authors would also like to acknowledge the support provided by Universiti Tun Hussein Onn Malaysia (UTHM) for their grant UTHM TIER 1, Grant No. H763. The authors would like to acknowledge the support provided by Ministry of Higher Education (MOHE) and Universiti Teknologi Malaysia (UTM) under Collaborative Research Grant (CRG), Grant No. 08G30 and 08G31.

**References:**

[1] C. Lee et al., "Soft robot review," Int. J. of Control, Automation and Systems, Vol.15, No.1, pp. 3-15, doi: 10.1007/s12555-016-0462-3, 2017.

[2] M. N. Ribuan, S. Wakimoto, K. Suzumori, and T. Kanda, "Omnidirectional soft robot platform with flexible actuators for medical assistive device," Int. J. Automation Technol., Vol.10, No.4, pp. 494-502, doi: 10.20965/ijat.2016.p0494, 2016.

[3] L. A. T. Al Abeach, S. Nefti-Meziani, and S. Davis, "Design of a Variable Stiffness Soft Dexterous Gripper," Soft Robotics, Vol.4, No.3, pp. 274-284, doi: 10.1089/soro.2016.0044, 2017.

[4] K. Batsuren and D. Yun, "Soft robotic gripper with chambered fingers for performing in-hand manipulation," Applied Sciences, Vol.9, No.15, 2967, doi: 10.3390/app9152967, 2019.

[5] I. D. Walker, "Continuous Backbone 'Continuum' Robot Manipulators," ISRN Robotics, Vol.2013, pp. 1-19, doi: 10.5402/2013/726506, 2013.

[6] J. Hughes, U. Culha, F. Giardina, F. Guenther, A. Rosendo, and F. Iida, "Soft manipulators and grippers: A review," Frontiers in Robotics and AI, Vol.3, doi: 10.3389/frobt.2016.00069, 2016.

[7] T. George Thuruthel, Y. Ansari, E. Falotico, and C. Laschi, "Control Strategies for Soft Robotic Manipulators: A Survey," Soft Robotics, Vol.5, No.2, pp. 149-163, doi: 10.1089/soro.2017.0007, 2018.

[8] E. W. Hawkes, L. H. Blumenschein, J. D. Greer, and A. M. Okamura, "A soft robot that navigates its environment through growth," Science Robotics, Vol.2, No.8, pp. 1-8, doi: 10.1126/scirobotics.aan3028, 2017.

[9] B. L. Conrad and M. R. Zinn, "Interleaved continuum-rigid manipulation: An approach to increase the capability of minimally invasive surgical systems," IEEE/ASME Trans. Mechatronics, Vol.22, No.1, pp. 29-40, doi: 10.1109/TMECH.2016.2608742, 2017.

[10] J. H. Hsiao, J. Y. Chang, and C. M. Cheng, "Soft medical robotics: clinical and biomedical applications, challenges, and future directions," Advanced Robotics, Vol.33, No.21, pp. 1099-1111, doi: 10.1080/01691864.2019.1679251, 2019.

[11] A. A. M. Faudzi, N. H. I. Mat Lazim, and K. Suzumori, "Modeling and force control of thin soft McKibben actuator," Int. J. Automation Technol., Vol.10, No.4, pp. 487-493, doi: 10.20965/ijat.2016.p0487, 2016.

[12] I. De Falco, M. Cianchetti, and A. Menciassi, "A soft multimodule manipulator with variable stiffness for minimally invasive surgery," Bioinspiration and Biomimetics, Vol.12, No.5, 056008, doi: 10.1088/1748-3190/aa7ccd, 2017.

[13] L. H. Blumenschein, L. T. Gan, J. A. Fan, A. M. Okamura, and E. W. Hawkes, "A Tip-Extending Soft Robot Enables Reconfigurable and Deployable Antennas," IEEE Robotics and Automation Letters, Vol.3, No.2, pp. 949-956, doi: 10.1109/LRA.2018.2793303, 2018.

[14] E. Y. Yarbasi and E. Samur, "Design and evaluation of a continuum robot with extendable balloons," Mechanical Sciences, Vol.9, No.1, pp. 51-60, doi: 10.5194/ms-9-51-2018, 2018.

[15] J. O. Alcaide, L. Pearson, and M. E. Rentschler, "Design, modeling and control of a SMA-actuated biomimetic robot with novel functional skin," Proc. of the 2017 IEEE Int. Conf. on Robotics and Automation (ICRA), pp. 4338-4345, doi: 10.1109/ICRA.2017.7989500, 2017.

[16] J. E. Bernth, A. Arezzo, and H. Liu, "A novel robotic meshworm with segment-bending anchoring for colonoscopy," IEEE Robotics and Automation Letters, Vol.2, No.3, pp. 1718-1724, doi: 10.1109/LRA.2017.2678540, 2017.

[17] A. Vandini, C. Bergeles, B. Glocker, P. Giataganas, and G. Z. Yang, "Unified Tracking and Shape Estimation for Concentric Tube Robots," IEEE Trans. on Robotics, Vol.33, No.4, pp. 901-915, doi: 10.1109/TRO.2017.2690977, 2017.

[18] J. Ha, F. C. Park, and P. E. Dupont, "Optimizing Tube Precurvature to Enhance the Elastic Stability of Concentric Tube Robots," IEEE Trans. on Robotics, Vol.33, No.1, pp. 22-37, doi: 10.1109/TRO.2016.2622278, 2017.

[19] A. K. Mishra, E. Del Dottore, A. Sadeghi, A. Mondini, and B. Mazzolai, "SIMBA: Tendon-driven modular continuum arm with soft reconfigurable gripper," Frontiers in Robotics and AI, Vol.4, 4, doi: 10.3389/frobt.2017.00004, 2017.

[20] Z. Zhang, J. Dequidt, J. Back, H. Liu, and C. Duriez, "Motion Control of Cable-Driven Continuum Catheter Robot Through Contacts," IEEE Robotics and Automation Letters, Vol.4, No.2, pp. 1852-1859, doi: 10.1109/LRA.2019.2898047, 2019.

[21] M. M. Tonapi, I. S. Godage, A. M. Vijaykumar, and I. D. Walker, "A novel continuum robotic cable aimed at applications in space," Advanced Robotics, Vol.29, No.13, pp. 861-875, doi: 10.1080/01691864.2015.1036772, 2015.

[22] I. A. Gravagne and I. D. Walker, "Manipulability, Force, and Compliance Analysis for Planar Continuum Manipulators," IEEE Trans. on Robotics and Automation, Vol.18, Issue 3, pp. 263-273, doi: 10.1109/TRA.2002.1019457, 2002.

[23] S. Tully, A. Bajo, G. Kantor, H. Choset, and N. Simaan, "Constrained filtering with contact detection data for the localization and registration of continuum robots in flexible environments," Proc. of the 2012 IEEE Int. Conf. on Robotics and Automation, pp. 3388-3394, doi: 10.1109/ICRA.2012.6225080, 2012.

[24] A. D. Marchese and D. Rus, "Design, kinematics, and control of a soft spatial fluidic elastomer manipulator," The Int. J. of Robotics Research, Vol.35, No.7, pp. 840-869, doi: 10.1177/0278364915587925, 2016.

[25] M. Hwang and D. S. Kwon, "Strong Continuum Manipulator for Flexible Endoscopic Surgery," IEEE/ASME Trans. Mechatronics, Vol.24, No.5, pp. 2193-2203, doi: 10.1109/TMECH.2019.2932378, 2019.

[26] A. A. Faudzi, N. I. Azmi, M. Sayahkarajy, W. L. Xuan, and K. Suzumori, "Soft manipulator using thin McKibben actuator," Proc. of the 2018 IEEE/ASME Int. Conf. on Advanced Intelligent Mechatronics (AIM), pp. 334-339, doi: 10.1109/AIM.2018.8452698, 2018.

[27] A. K. Mishra, A. Mondini, E. Del Dottore, A. Sadeghi, F. Tramacere, and B. Mazzolai, "Modular continuum manipulator: Analysis and characterization of its basic module," Biomimetics, Vol.3, No.1, 3, doi: 10.3390/biomimetics3010003, 2018.

**Name:**
Mohamed Tahir Shoani

**Affiliation:**
Ph.D. Student, Universiti Tun Hussein Onn Malaysia (UTHM)

**Address:**
Parit Raja, Batu Pahat, Johor 86400, Malaysia

**Brief Biographical History:**
2007-2011 Computer Teacher, The American International School in Abu Dhabi (AISA)
2015-2017 Lecturer, Cihan University
2017- Ph.D. Student, UTHM

**Main Works:**
• "Face Recognition Based Security Robot Incorporating Omnidirectional Vision," Master's thesis, Universiti Teknologi Malaysia, 2015.

**Name:**
Mohamed Najib Ribuan

**Affiliation:**
Senior Lecturer, Universiti Tun Hussein Onn Malaysia (UTHM)

**Address:**
Parit Raja, Batu Pahat, Johor 86400, Malaysia

**Brief Biographical History:**
2001- Service Engineer, Endress+Hauser (M) Sdn. Bhd.
2003- Instructor Engineer, Kolej Universiti Teknologi Tun Hussein Onn (KUiTTHO)
2007- Postgraduate, Mechanical and System Engineering, Newcastle University
2008- Lecturer, UTHM
2012- Postgraduate, Department of Intelligent Mechanical Systems, Okayama University
2016- Senior Lecturer, Department of Mechatronic and Robotic, UTHM

**Main Works:**
• "New Pneumatic Rubber Leg Mechanism for Omnidirectional Locomotion," Int. J. Automation Technol., Vol.8, No.2, pp. 222-230, 2014.

**Membership in Academic Societies:**
• Institute of Electrical and Electronics Engineers (IEEE)
• Board of Engineers Malaysia (BEM)

**Name:**
Ahmad Athif Mohd Faudzi

**Affiliation:**
Professor, Universiti Teknologi Malaysia (UTM)

**Address:**
Skudai, Johor 81310, Malaysia

**Brief Biographical History:**
2006-2011 Lecturer, UTM
2011-2015 Senior Lecturer, UTM
2015- Associate Professor, UTM
2015- Visiting Research Fellow, Tokyo Institute of Technology
2018- CEO at Faculty Program Fellow, Ericsson Malaysia Sdn. Bhd.
2019- Director, Centre for Artificial Intelligence and Robotics (CAIRO)
2021- Professor, UTM

**Main Works:**
• "Trends in Hydraulic Actuators and Components in Legged and Tough Robots: A Review," Adv. Robot., Vol.32, No.9, pp. 458-476, 2018.
• "Long-Legged Hexapod Giacometti Robot Using Thin Soft McKibben Actuator," IEEE Robotic Automation Letter, Vol.3, No.1, pp. 100-107, 2018.
• "Structural Analysis of Portable Repositioning Equipment for Bedridden Patients," J. Teknologi, Vol.72, No.2, pp. 89-92, doi: 10.11113/jt.v72.3890, 2015.

**Membership in Academic Societies:**
• Institute of Electrical and Electric Engineers (IEEE) Robotics and Automation Society (RAS)
• Institute of Electrical and Electric Engineers (IEEE) Control Systems Society (CSS)
• Institution of Engineering and Technology (IET)
• Asian Control Association (ACA)